IEEE Access
Multidisciplinary | Rapid Review | Open Access Journal

Received 2 March 2024, accepted 9 April 2024, date of publication 22 April 2024, date of current version 3 May 2024.

Digital Object Identifier 10.1109/ACCESS.2024.3392272

RESEARCH ARTICLE

A Simplified Texture Modeling Using a Physical and Perceptual Rule-Based Approach

KEISUKE TOZUKA[1], (Graduate Student Member, IEEE), AND HIROSHI IGARASHI[2], (Member, IEEE)

[1]Department of Electronic System Engineering, Tokyo Denki University, Adachi City, Tokyo 120-8551, Japan
[2]Department of Electrical and Electronic System Engineering, Tokyo Denki University, Adachi City, Tokyo 120-8551, Japan

Corresponding author: Keisuke Tozuka (k.tozuka@crl.epi.dendai.ac.jp)

This work was supported in part by the Research Institute for Science and Technology, Tokyo Denki University, Japan, under Grant Q23DS-02.

This work involved human subjects or animals in its research. Approval of all ethical and experimental procedures and protocols was granted by the Human Life Ethics Committee at Tokyo Denki University.

ABSTRACT In this paper, a method for creating texture models with physical significance using a parametric equalizer (PEQ)-based approach is presented. The model is based on the frequency, amplitude, bandwidth, and noise ratio corresponding to texture profiles. Additionally, the method simplifies the modeling process by enabling the selective omission of imperceptible roughness layers based on human tactile thresholds. The effectiveness of the simplified model was validated through subjective evaluations comprising both absolute and relative assessments. The results confirmed that layers with imperceptible roughness could be excluded without compromising perceived similarity, streamlining the texture modeling process. Regression analysis revealed that PEQ parameters reflect physical interactions in tactile sensations, such as the relationship between texture roughness and vibration amplitude. This study contributes to haptic texture modeling by offering a method that efficiently reproduces actual textures and mirrors the fundamental physical principles of touch. The findings hold promise for applications in texture authoring and material selection, indicating potential advancements in the development of more intuitive and physically transparent texture models.

INDEX TERMS Haptic rendering, texture, vibration, tactile, force feedback.

I. INTRODUCTION

When probing the surface of an object with a hard tool such as a pen, humans can perceive the texture profiles of the surface. This perception is enabled by vibrations transmitted to the tool during its interaction with the surface [1]. This principle has been used to reproduce textures using vibrators [2], [3]. The contributions of Bensmaia et al. highlighted the significance of spectral similarity in vibrations [4], leading to the prevalent approach of generating vibrations through filtering [5], [6]. This method involves measuring the interaction vibrations of actual object surfaces and reproducing their spectra using digital filters. Romano et al. extended this technique to an automatic filter design system [7]. Moreover, Culbertson et al. achieved reproduction with fewer filter orders [8]. There have also been some efforts to accommodate inhomogeneous textures [9], [10], [11], making the filtering method one of the most refined texture reproduction methods available today.

A significant recent advancement is the ability to create new textures from texture models. These include predicting vibrations of unmeasured textures [12], [13], [14], texture authoring [15], and texture suggestions based on user preferences [16]. In particular, texture generation systems based on user preferences can potentially promote the development of new materials in the surface processing industry [17]. Kurita et al. provided a digital tactile design tool based on images [18]. However, this is still a challenging topic. Existing texture authoring systems are primarily structured around subjective axes of roughness and hardness. It is difficult for subjective evaluation to describe the details of texture profiles.

The associate editor coordinating the review of this manuscript and approving it for publication was Claudia Raibulet.

In this paper, a method for generating texture models that can be associated with texture profiles is introduced. From a physical perspective, object surfaces are composed of multiple layers of roughness. From a perceptual viewpoint, reproducing sufficiently small roughness can be redundant. By integrating both perspectives, our model aims to facilitate the challenging theme of texture authoring. The parameters constituting our texture model are affected by physical interactions. Physics-guaranteed texture models can be useful in developing more specific texture authoring systems. In addition, our method can be used to simplify the model through physical and perceptual rules.

A. PHYSICALLY TRANSPARENT TEXTURE MODELS

The interaction vibrations arising from tool collisions with specific surface patterns contain various vibration characteristics corresponding to the texture profiles. Since it is impractical to model all these interaction vibrations, a texture authoring system has been proposed [15]. This system allows users to determine the desired texture profile and generates a texture model based on the determination. However, due to the complexity of texture modeling techniques, the proposed authoring systems were unable to configure detailed texture profiles. Modeling techniques require versatility to accommodate all types of interaction vibrations. In previous modeling works, filters with numerous coefficients were adopted for versatility and reproducibility [7], [8]. These filter coefficients do not have physical meaning.

According to texture authoring teams, these numerous filter coefficients make physical interpretation difficult [15], [16]. This means that the previous texture model lacks physical transparency. Therefore, they used subjective-based roughness and hardness data selected by the subjects in advance. Although actual textures include multiple roughness layers, representing the roughness of multiple layers using subjective roughness is difficult. Additionally, the randomness of texture patterns plays a crucial role in texture perception [19], but this has not been included in subjective-based approaches.

To create an advanced authoring system selectable for these textures, the texture model must include physical meaning. Although physical simulation generates vibrations following physical procedures, this method challenges real-time performance [20]. However, even without adhering to physical procedures, the vibration spectrum itself offers valuable insight into texture profiles [21], [22]. The important information lies in the spectral peaks, i.e., parameters such as the fundamental frequency that characterizes those peaks. A modeling technique that utilizes the characteristics of these peaks can provide an authoring system capable of detailed configurations.

B. REPRODUCING ROUGHNESS LAYERS

In the industrial field, the roughness is defined as the arithmetic mean roughness (Ra) and maximum height (Ry). This has two perceived roughness layers: macroroughness and microroughness [23], [24]. Multiple peaks in the measured vibration spectrum suggest the presence of multiple roughness layers. Among these multiple peaks, some vibrations cannot be detected by humans [25]. The design of a texture model can be simplified by discerning which elements are significant and which are not significant for humans [26], [27].

Compression according to perceptual rules was proposed in the field of vibrotactile transmission [28], [29]. The ST-SIM evaluation function proposed by Hassen et al. considers the detection threshold, achieving both reproducibility and signal compression [30]. Their procedure can also be used to simplify the texture model. However, this compression procedure does not follow physical rules. High-frequency vibrations (fine roughness) only become vibrations beyond the threshold with sufficient probing speed and force. The removal of vibrations below the threshold can cause new frequency components to appear when the probing speed and force are suddenly high. This means that the texture model is partially missing information. Texture models with partially missing features are not suitable for machine learning applications. Naturally, this also negatively impacts texture authoring systems. In our approach, textures are identified by the number of layers of roughness via peak detection from the measured spectrum. Then, for each layer of roughness, the decision is made whether to reproduce the layer based on the perceptual threshold.

C. EQUALIZERS AND TEXTURE VIBRATIONS

The texture profile affects the prominent peaks in the vibration spectrum, and the number of peaks indicates the number of roughness layers. Therefore, an approach needs to be developed to determine the peak characteristics that change according to the probing speed and force.

We focused on employing an equalizing system for this purpose. An equalizer consists of a combination of narrowband filters and gains. The fundamental frequency and bandwidth of the narrowband filter and the gain represent the characteristics of the peaks. When representing multiple peaks, a parametric equalizer (PEQ) constructed with multiple equalizers is suitable. Few efforts have been made to date, and equalizer-based texture reproduction has yet to be proposed. In the vibrotactile sensations field, equalizing has primarily been used for inverse filtering to eliminate the effects of resonance characteristics [31]. Alma et al. reported that bandwidth-limited white noise can replace textural stimuli [32]. Their study is in the investigation phase, and they are not yet at the stage of proposing a texture model. Therefore, based on their reported results, we employed a PEQ-based modeling method that includes multiple roughness layers.

General approaches involve constructing an optimal filter through a predictive loop that minimizes the spectral matching function. This approach is not applicable when reproducing individual peaks. To construct a PEQ from measured vibration spectra, a modeling method based on peak analysis is necessary. In this paper, a system that can

be used to automatically design a PEQ by analyzing the peaks of the measured vibrations is introduced. Additionally, we present and discuss a model simplification process based on roughness layers and perceptual thresholds.

II. DATA COLLECTION

In this section, the procedure for collecting probing vibration data from actual object surfaces is described. The content of this section includes an overview of the proprietary recording device, data collection methods, and device controls. In addition, the selection criteria for texture samples and the procedures for processing the recorded signals are detailed.

A. DEVICE

The mechanism of the recording device is akin to that of a record player, featuring a turntable and a contactor, as shown in Fig. 1. The device is structured with an independent dual-layer design, placing the turntable and contactor on the upper part, while the motor driving the turntable, power supply, and microcontroller are housed in the lower part. This design effectively prevents vibrations from the speed-controlled motor from infiltrating the recorded data. Hence, the turntable and the driving motor are coupled with magnetic coupling, maintaining a 10-mm separation.

The 3D-printed ABS resin contactor is equipped with an Analog 'Devices ADcmXL3021 accelerometer, and a steel ball with chrome plating is used at the contact point. The spheres were sized with a diameter of 3 mm to interact with the textured sample [33]. The turntable and contactor are powered by the Maxon Motor gearless motor DCX32L. The distance from the contact point to the motor shaft is 30 mm, which is capable of exerting a maximum vertical force of 4.0 N. The rotation speed can reach 7260 rpm, covering the entire range of tool-material interactions. A disturbance observer (DOB) and reaction torque observer (RTOB) proposed by Ohnishi et al. [34] are used for force control, allowing for sensorless control of the contact force. The observers also applied speed control, enabling the turntable to rotate at the commanded speed. An ARM microcontroller F767ZI entirely manages the motor control at a sampling rate of 5 kHz.

B. TEXTURE SURFACE

Seven types of texture samples, including metals, fabrics, animal-based materials, plastics, and wood, were used to evaluate the modeling and rendering process (Fig. 2). Two fabrics were selected to be perceived similarly in the subjective evaluation. Two types of plastics, *PVC* and *wall paper*, were selected to investigate perceptual differences in surface morphology. All texture samples were cut to a diameter of 120 mm. During recording, texture samples were secured to an aluminum turntable of the same diameter using screws. Except for *MDF*, which was 4 mm thick, the other six textures were mounted on acrylic plates with double-sided tape. This process was performed to match the thicknesses.

C. RECORDING

Vibration data were recorded through the EVAL-ADCM evaluation board at 22.704 kHz for 1 second. Vibration data corresponding to the two conditions of force and speed were recorded. Once the data were saved to the specified folder on a PC, the following measurement conditions were used according to the number of saved files. Regarding the measurement conditions, researchers have previously determined the range of speeds and forces based on haptic exploration by humans [8]. This range was investigated experimentally, reflecting its dependence on the experimental environment. In our experimental environment, seven velocity steps up to 350 mm/s and seven force steps up to 3.5 N were needed. The recorded data were downsampled to 5 kHz, and a high-pass filter at 10 Hz was applied.

III. MODELING

Fig. 3 illustrates the process of PEQ construction from the recorded vibrations. Four essential elements are required to construct a PEQ: the amount of white noise, the fundamental frequency, the bandwidth, and the amplitude. These elements are the vibration characteristics that describe the influences of the texture profiles. The amount of white noise can be used to determine the degree of randomness. Regardless of the texture, achieving a perfectly clean sine-wave grid is rare. Most textures have some degree of randomness, which can be represented across all bands by adjusting the amount of white noise. The fundamental frequency can be used to explain the spatial wavelength of the texture, typically defined as $f = v/\lambda$. v is the velocity, and λ is the wavelength, indicating multiple spatial wavelengths if multiple frequencies are present. Furthermore, the surface hardness can alter the transient acceleration frequency [35]. The bandwidth indicates the variation in fundamental frequency, representing the randomness of the spatial wavelength [19]. The amplitude is directly related to the vibration energy arising from collisions between the probe and the surface bumps [20]. The depth of probe penetration, influenced by the bump depth, affects probe displacement [36]. The collision force increases with the hardness of the probe and object. Thus, the amplitude is affected by the hardness and bump depth [37].

Multiple narrow-band filters and gains are required to express roughness layers with an equalizer. This combination of multiple narrow-band filters and gains is used as a PEQ in acoustics. The PEQ formula is expressed as follows:

$$\hat{a}(z) = G_w a_w(z) + H_{\mathrm{PEQ}}(z) a_w(z) \tag{1}$$

Here, $a_w(z)$ represents the original white noise signal. The composite signal is the sum of the signal limited by $H_{\mathrm{PEQ}}(z)$ and the noise amplified by the noise gain G_w. $H_{\mathrm{PEQ}}(z)$ is defined as follows:

$$H_{\mathrm{PEQ}}(z) = \sum_{i=1}^{m} G_i(z) H_i(z) \tag{2}$$

where $\boldsymbol{G}_m$ is the peak gain, and $\boldsymbol{H}_m(z)$ is the bandpass filter. Both increase with the number of peaks m, and

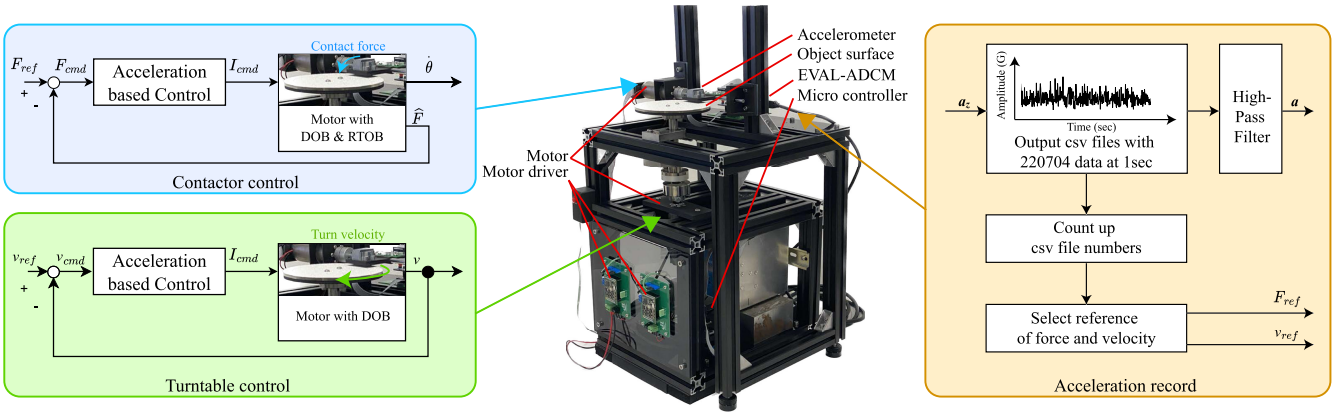

FIGURE 1. A vibration recording device. The rotational speed and normal force that operate the device are controlled on a microcontroller at a 5 kHz sampling rate. The measured vibrations are stored on a PC database in CSV format.

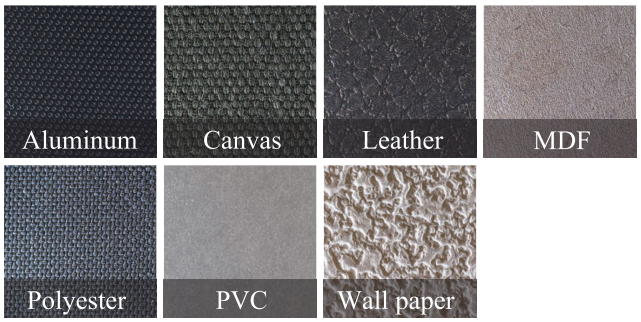

FIGURE 2. Seven texture samples used for validation. Each sample has different physical properties and was used to evaluate the texture reproduction methods in this paper. Surface images were taken with a Nikon Z6 lens (TAMRON SP AF90 mm F/2.8 Di MACRO1:1). The captured images were cropped to 15 mm in height and width.

peak reproduction is achieved through band limitation and amplification (Fig. 4). The characteristics $\boldsymbol{Q}_m$ of $\boldsymbol{H}_m(z)$ are determined by the fundamental frequency $\boldsymbol{f}_m$ and the bandwidth $\boldsymbol{B}_m$. Thus, the parameters needed to construct a PEQ are obtained from the peak information, which is analyzed after peak detection.

After a fast Fourier transform (FFT) is performed, the recorded texture dataset was initially smoothed with a Gaussian filter with a standard deviation of $\sigma = 30$. Peaks were then detected using a hill-climbing algorithm on the smoothed spectrum. The detected peak amplitudes and frequencies become the peak gain $\boldsymbol{G}_m$ and the fundamental frequency $\boldsymbol{f}_m$ of the PEQ. The peak gain $\boldsymbol{G}_m$ is the ratio of the peak amplitude $\boldsymbol{A}_m$ to the average amplitude of the original white noise. Gaussian fitting was applied to the detected peaks to estimate their bandwidths using the PEQ bandwidth $\boldsymbol{B}_m$. The average amplitude in a band sufficiently distant from the peaks (e.g., 2 k to 2.5 kHz) was defined as the noise amount A_w, and G_w was calculated via the same process used to obtain $\boldsymbol{G}_m$.

Please note that this PEQ is very sensitive to the quality of the acquired signals. It is necessary to ensure that the accelerometer is low-noise, and that sufficient data is secured with constant force and speed. In addition, we are addressing this issue signal-processing-wise. Assuming that the number of peaks correlates with the number of roughness layers, even if the number of detected peaks varies with recording conditions, the number of roughness layers should not fluctuate within the texture model. Therefore, peak detection was performed in descending order from the data with the most potent force and the fastest speed to maintain peak identity under various conditions. The number of peaks detected in the first dataset was fixed to the maximum peak number. The frequencies of the detected peak and adjacent data were compared to determine the peak with the frequency closest to that of the same peak. To prevent mixing, we limited the comparison range to half the frequency difference between previously identified adjacent peaks. If a peak was not detected in subsequent data, the fundamental frequency of the previous peak data was inherited, and only the bandwidth and amplitude were updated. This inheritance system addresses sudden peak detection errors and peak disappearances at low speeds.

IV. VIBRATION PROPERTY

This section aims to demonstrate that the created texture models possess physical transparency. As explained in Section III, the parameters of PEQ are influenced by the texture profile and the interactions involved. By examining the modeled PEQ parameters, details of the interaction of the texture samples are predicted. Furthermore, by analyzing the response to the force and speed, measurement or modeling errors are considered.

A. MULTIPLE REGRESSION MODEL

It is essential to investigate the response to the force and speed to understand the relationship between the texture profiles and these PEQ parameters P (such as the frequency, amplitude, or bandwidth). The response of each parameter might depend on the speed, force, or their interaction. Therefore, we apply the following multiple regression

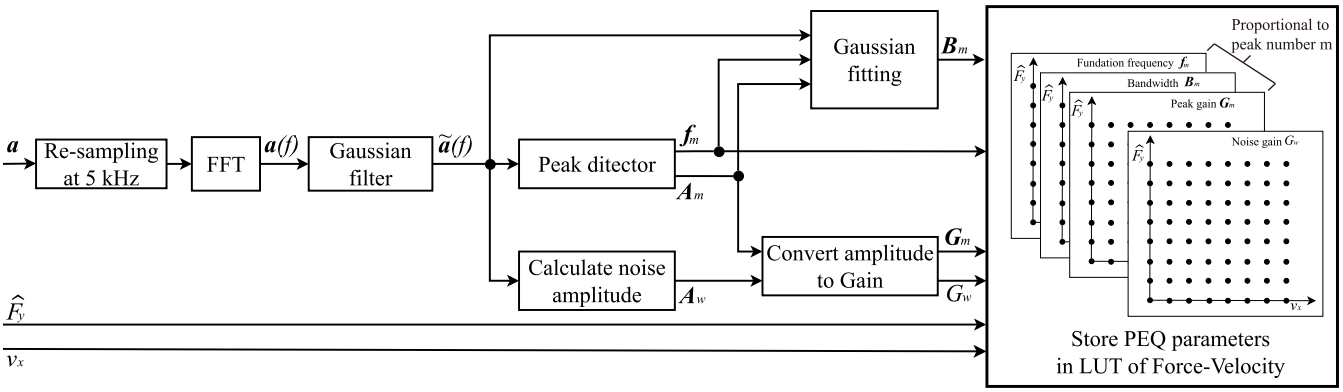

FIGURE 3. The acquired vibration signal is downsampled, the FFT is applied, and the result is further smoothed. Peak detection is performed on the smoothed spectrum, and information about the detected peaks is acquired. The acquired peak information about the probing force and velocity during vibration recording is stored. Notably, the amount of data stored depends not only on the number of force and velocity steps during the recording but also on the number of peaks detected.

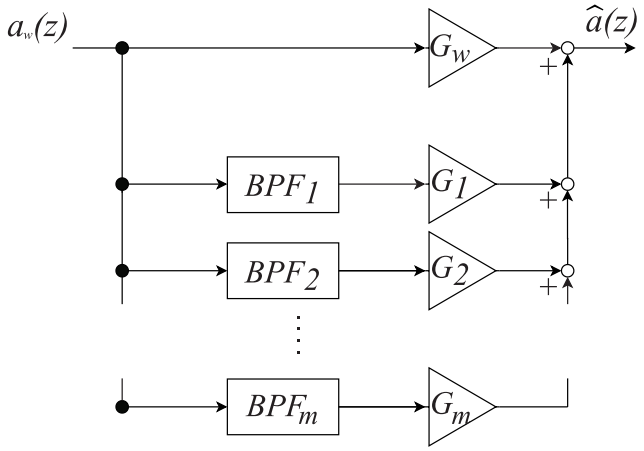

FIGURE 4. Block diagram of PEQ. Band-pass filters limit the bandwidth and are then amplified by gains. The combinations of band-pass filter and gain vary depending on the number of peaks.

formula to examine the influence on each parameter P:

$$P = \beta + \alpha_1 v + \alpha_2 \hat{F} + \alpha_3 v\hat{F} \tag{3}$$

In this equation, P is a generic PEQ parameter, β is the intercept, α_1 is the regression coefficient for speed, α_2 is for force, and α_3 is for the interaction between speed and force. The appropriate regression models are selected for each PEQ parameter by checking the significance of each regression coefficient.

B. REGRESSION MODEL FIT LEVEL

Table 1 lists the effectiveness of each regression model excluding the intercept for each PEQ parameter on different peaks. It includes the multiple correlation R, the adjusted coefficient of determination R^2, and each regression model's significance level p. Intercepts are significant if they are above zero, making them significant about frequencies and bandwidths. If there is no significant difference, it is only because the value of amplitudes and bandwidths in most minor combinations of the speed and force was small.

By averaging the R^2 values for each PEQ parameter, $\bar{R}^2(n) = 0.68$, $\bar{R}^2(f) = 0.40$, $\bar{R}^2(a) = 0.88$, and $\bar{R}^2(b) = 0.2$. Except for $\bar{R}^2(b)$, these values indicate a good fit ($\bar{R}^2 > 0.4$), showing that the regression models were adequate to explain the PEQ parameters. Only the intercept might be affected by the low value of $\bar{R}^2(b)$.

C. PHYSICAL INTERPRETATION OF THE MODEL

Before examining individual peaks, it is necessary to identify the overall trends. The support ratings and the averages of the coefficients are shown in Table 2 and were calculated based on the significance of each PEQ parameter ($p < 0.05$).

The physical implications of the regression model are discussed in Table 2. From this table, α_1 of the noise gain showed a negative trend. The noise gain is the overall randomness of the surface. The noise gain shows a strong decrease in the velocity response, probably due to an increase in the signal at the primary spatial wavelengths. On the other hand, the bandwidth did not respond to velocity or force due to the randomness of the primary spatial wavelengths. Since the bandwidth only responds to the intercept and not to either velocity or force, it becomes statistically insignificant in the analysis.

The fundamental frequency of the peaks shows the individual responses to the speed and force, although the support rating is relatively low. This result might be due to the variation in individual peaks across textures. For example, in *canvas*, the lower frequency peak increases with speed, while the others do not. This trend suggests that at higher speeds, fewer interactions occur due to hopping over larger bumps. To confirm this hypothesis, the spectral centroid SC was calculated as follows:

$$SC = \frac{\sum_{i=1}^{m} \{G_i(z)\}^2 F_i(z)}{\sum_{i=1}^{m} \{G_i(z)\}^2} \tag{4}$$

SC shows a frequency trend across the spectrum.

SC can be applied similarly to a multiple regression model, and a strong increasing trend appeared for the velocity (Fig. 5). The frequency trend of the entire spectrum follows

TABLE 1. Validity list for each regression model at each PEQ parameter by peak. The significance levels are defined as $p < 0.05$ for *, $p < 0.01$ for **, and $p < 0.001$ for ***. The intercept coefficient β is excluded from this table.

Noise gain					Peak	Frequency					Amplitude					Bandwidth				
R	R^2	α_1	α_2	α_3	m	R	R^2	α_1	α_2	α_3	R	R^2	α_1	α_2	α_3	R	R^2	α_1	α_2	α_3
Aluminum																				
0.95	0.90	***	n.s.	**	1	0.99	0.98	***	n.s.	n.s.	0.95	0.89	***	n.s.	*	0.93	0.85	***	n.s.	n.s.
					2	0.49	0.19	*	n.s.	n.s.	0.92	0.84	***	n.s.	**	0.93	0.85	***	n.s.	n.s.
Canvas																				
0.72	0.49	n.s.	n.s.	*	1	0.97	0.94	***	n.s.	n.s.	0.92	0.83	***	*	***	0.90	0.81	***	n.s.	n.s.
					2	0.69	0.44	n.s.	n.s.	**	0.93	0.86	n.s.	***	***	0.20	-0.02	n.s.	n.s.	n.s.
					3	0.50	0.20	n.s.	n.s.	*	0.90	0.79	n.s.	n.s.	***	0.25	0.00	n.s.	n.s.	n.s.
Leather																				
0.92	0.84	***	n.s.	n.s.	1	0.65	0.39	n.s.	*	n.s.	0.98	0.97	***	**	n.s.	0.42	0.12	*	n.s.	n.s.
					2	0.64	0.37	*	n.s.	n.s.	0.96	0.91	***	**	***	0.33	0.05	n.s.	*	n.s.
					3	0.53	0.24	n.s.	n.s.	n.s.	0.95	0.90	***	**	***	0.24	-0.00	n.s.	n.s.	n.s.
					4	0.60	0.32	n.s.	*	n.s.	0.97	0.93	***	**	***	0.18	-0.03	n.s.	n.s.	n.s.
MDF																				
0.89	0.79	***	n.s.	n.s.	1	0.60	0.31	**	n.s.	n.s.	0.99	0.97	***	**	**	0.55	0.26	**	*	n.s.
					2	0.65	0.38	**	n.s.	n.s.	0.96	0.93	***	*	***	0.25	0.00	n.s.	n.s.	n.s.
					3	0.72	0.48	n.s.	***	n.s.	0.98	0.95	***	*	***	0.28	0.02	n.s.	n.s.	n.s.
					4	0.63	0.35	*	n.s.	n.s.	0.95	0.90	***	n.s.	*	0.35	0.06	n.s.	*	n.s.
Polyester																				
0.70	0.46	**	n.s.	n.s.	1	0.33	0.05	n.s.	n.s.	n.s.	0.78	0.59	*	**	n.s.	0.13	-0.05	n.s.	n.s.	n.s.
					2	0.53	0.23	n.s.	n.s.	n.s.	0.92	0.84	***	n.s.	**	0.36	0.07	n.s.	n.s.	n.s.
					3	0.70	0.45	***	*	n.s.	0.91	0.81	***	*	**	0.26	0.00	n.s.	n.s.	n.s.
					4	0.54	0.24	n.s.	*	n.s.	0.90	0.81	***	n.s.	**	0.13	-0.05	n.s.	n.s.	n.s.
PVC																				
0.90	0.81	***	*	*	1	0.76	0.55	n.s.	***	n.s.	0.91	0.81	***	n.s.	n.s.	0.32	0.04	n.s.	n.s.	n.s.
					2	0.78	0.58	***	n.s.	n.s.	0.97	0.94	***	n.s.	**	0.23	-0.01	n.s.	n.s.	n.s.
					3	0.26	0.01	n.s.	n.s.	n.s.	0.96	0.91	***	n.s.	n.s.	0.20	-0.03	n.s.	n.s.	n.s.
Wall paper																				
0.73	0.50	***	*	n.s.	1	0.96	0.91	n.s.	n.s.	***	0.97	0.93	***	n.s.	***	0.82	0.65	n.s.	**	n.s.
					2	0.79	0.59	***	n.s.	n.s.	0.98	0.95	***	**	***	0.55	0.25	n.s.	n.s.	n.s.
					3	0.51	0.21	n.s.	n.s.	n.s.	0.97	0.95	***	***	***	0.63	0.36	n.s.	n.s.	n.s.
					4	0.38	0.08	n.s.	*	n.s.	0.97	0.93	***	**	***	0.37	0.08	n.s.	n.s.	n.s.
					5	0.64	0.37	n.s.	n.s.	n.s.	0.93	0.85	*	*	***	0.93	0.85	*	*	***

TABLE 2. Average of the support and regression coefficients of the regression model for each parameter of the PEQ. Support is high for any significant difference at any peak.

PEQ param	Support rating			Average of coeff		
	α_1	α_2	α_3	α_1	α_2	α_3
Noise gain	85.7	14.3	42.9	-5.7×10^{-8}	-1.0×10^{-7}	1.3×10^{-10}
Frequency	40.0	32.0	8.0	1.6×10^{-1}	6.0×10^{-3}	1.7×10^{-6}
Amplitude	92.0	72.0	88.0	4.0×10^{-4}	-1.7×10^{-5}	1.3×10^{-7}
Bandwidth	24.0	20.0	4.0	-2.6×10^{-4}	-5.9×10^{-6}	1.3×10^{-8}

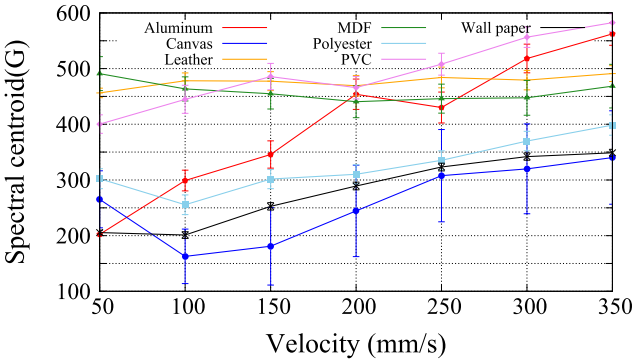

FIGURE 5. Response of the spectral centroid *SC* to the probing speed. The plot is an average between the different force conditions at the same speed conditions. The error bar is its standard deviation.

the relationship between spatial frequency and probing speed, but some peaks do not. In other words, it is not a measurement or peak detection error but rather the observed hopping effect.

The amplitude responds to the speed, force, and their interaction, although it proportionately decreases with the force. This trend might be due to the damping effect of higher forces on hopping, which reduces the amplitude. The correlation $R > 0.6$ between *SC* and amplitude supports this hypothesis, indicating a relationship between the roughness and the response to the amplitude and speed. These findings suggest that the proposed texture model can be used to explain the physical interactions on the surfaces. Future work could be conducted to involve a regression model for textures with known roughness and hardness values, linking physical texture properties directly to the model parameters.

V. MODEL SIMPLIFICATION

In the previous section, we established that the constructed texture models can reflect the physical interactions inherent to the tactile sensations. In this section, we describe the simplification process of these texture models, evaluating

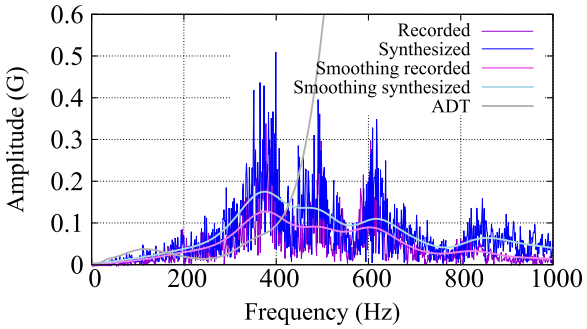

(a) Before simplification

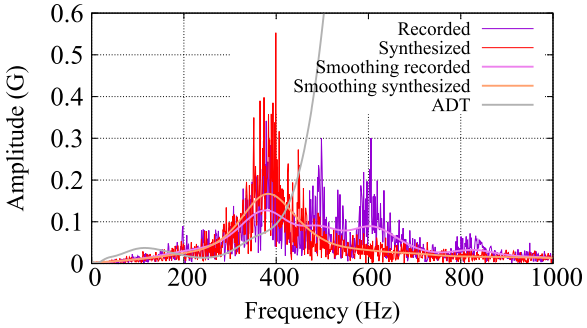

(b) After simplification

FIGURE 6. Comparison of the vibration spectra with the ADT. (a) is the case where all peaks are reproduced. (b) is the case where the peaks below the ADT are reduced. Spectra of the *canvas* are shown as an example.

the feasibility of selectively eliminating the roughness layer based on a perceptual threshold.

A. SIMPLIFICATION METHOD

Hassen et al. developed a method for compressing vibrotactile signals based on human perceptual thresholds [29]. While many researchers have investigated the perceptual threshold in terms of displacement [25], general vibrotactile display works use acceleration.

For this purpose, Hassen et al. described converting displacement-based perceptual thresholds into acceleration detection thresholds (ADT). Given a displacement $x(t)$ with amplitude a oscillating over time t, the acceleration $\ddot{x}$ can be described as follows:

$$\ddot{x} = -a\omega^2 x(t) \tag{5}$$

where ω represents the angular frequency of vibration. The ADT was calculated using this equation unit of G and compared with the amplitude of the PEQ. If the amplitude of each peak in every force and speed condition is below the ADT, the applicable peaks (roughness layers) are excluded from the texture model (Fig. 6).

B. SIMPLIFICATION RATE AND QUALITY

Some researchers have adopted the goodness fitting coefficient (GFC) to evaluate the similarity of vibration spectra [33], [38]. This function was initially used to assess the similarity of the light spectra. The *GFC* is an adaptation of the cosine similarity tailored for spectral evaluation without considering the sign [39], as defined by the following expression:

$$GFC = \frac{|\sum_i \hat{S}_o(f_i) S_o(f_i)|}{\sqrt{|\sum_j [\hat{S}_o(f_j)]^2|}\sqrt{|\sum_k [S_o(f_k)]^2|}} \tag{6}$$

A *GFC* value above 0.9 indicates high reproduction accuracy. Table 3 lists the degree of peak reduction and the change in the *GFC* for each texture. The *GFC* remains nearly unchanged for minimal peak reductions, such as in the case of *canvas*, where the difference is less than 0.01. The number of reduced peaks also impacts the *GFC*. The amplitude over the ADT curve was required to be larger at higher frequencies. Therefore, in this verification, the removed peaks were all more frequent. In other words, they were fine bumps. For example, in fabrics, only the roughness of the weave was presented, not the texture of the fibers, due to tool tip size limitations. The result excludes specific layers of the roughness based on the perceptual thresholds, suggesting the judgment of necessary roughness layers in texture authoring.

TABLE 3. A list of the degree of reduction in the number of peaks and the change in the spectral matching evaluation. A reduction of one peak reduces the number of the PEQ parameters by three. The minimum configuration is four parameters combined with the noise gain.

	Before simplify → After simplify	
Texture	peak number	Similarity *GFC*
Aluminum	peak number: 2 → 1	*GFC*: 0.88 → 0.76
Canvas	peak number: 3 → 1	*GFC*: 0.82 → 0.82
Leather	peak number: 4 → 1	*GFC*: 0.91 → 0.83
MDF	peak number: 4 → 1	*GFC*: 0.97 → 0.93
Polyester	peak number: 4 → 2	*GFC*: 0.92 → 0.90
PVC	peak number: 3 → 1	*GFC*: 0.93 → 0.83
Wall paper	peak number: 4 → 3	*GFC*: 0.84 → 0.80

VI. RENDERING

In this section, we discuss the system for rendering texture vibrations in response to varying probing speeds and forces. The vibrations are rendered on a virtual surface using a cable-linked force feedback device. The device's motor movements are monitored by a microcontroller, which drives the PEQ parameter models. The models are interpolated, and the PEQ parameters generate the texture vibrations (Fig. 7).

A. FORCE FEEDBACK

To present the target texture, the model must include the interaction forces and speeds of the operator. Pen-arm-based force-feedback devices, such as the Phantom Omni device, are widely used for such applications [40], [41], [42]. Although this device is easy to install in experimental setups, it is unsuitable for presenting a wide range of workspaces and strong forces. The arm frames also suppress vibrations. This limitation is a standard issue for robust arm-type devices.

In our approach, the cable-linked force feedback device generates force by pulling cables [43] with the two motors to

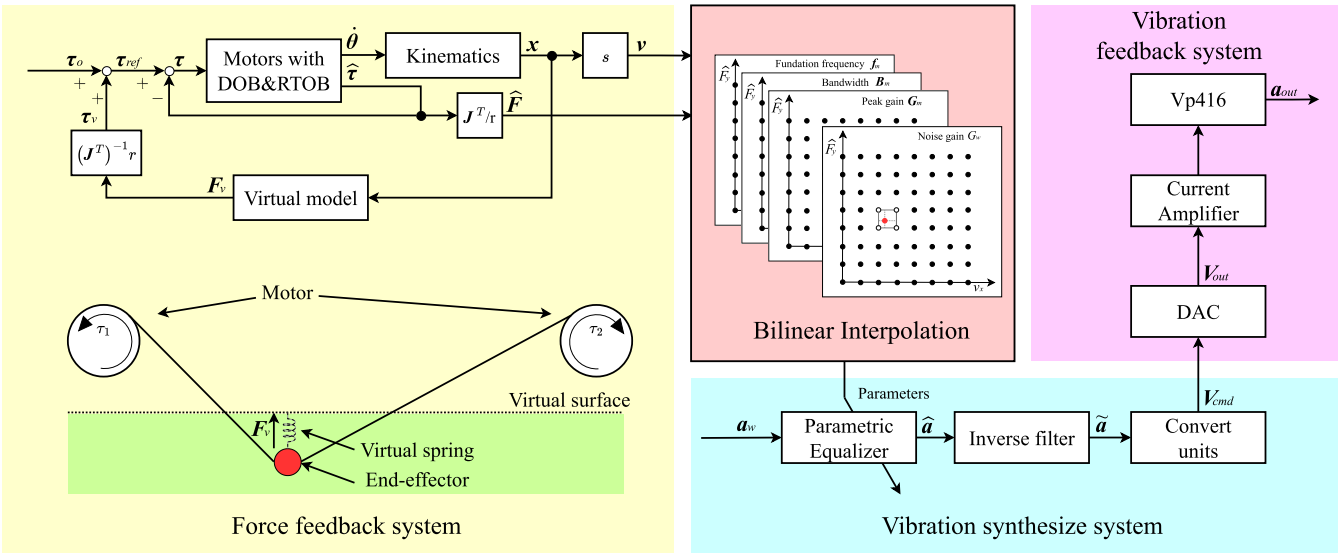

FIGURE 7. A cable-linked force feedback device provides the reaction force output on the virtual surface. When the operator manipulates this device, the tangential velocity and normal force are input to the texture model. If these velocities and forces are not on the recording data point, they are complemented by bilinear completion. With each PEQ parameter determined by completion, a PEQ can synthesize texture vibrations.

provide the reaction force. The position $\boldsymbol{x}$ of an end effector can be estimated by solving the kinematics using the rotation angles of the two motors. This position $\boldsymbol{x}$ is used to calculate the velocity v, input into the texture model, and compute the interaction with the virtual surface. The virtual surface is simplified as a spring model from which the reaction force $\boldsymbol{F_v}$ is calculated. The inverse Jacobian matrix converts the reaction force $\boldsymbol{F_v}$ into the output torque $\boldsymbol{\tau}_v$ for each motor. The operator torque $\hat{\boldsymbol{\tau}}$ applied at the motors is computed by the RTOB. This torque $\hat{\boldsymbol{\tau}}$ is converted back into the force $\hat{\boldsymbol{F}}$ applied by the operator on the surface through the Jacobian matrix and is input into the texture model.

B. MODEL INTERPOLATION

The PEQ parameters are linked with the forces and speeds during vibration recording. Similarly, it is necessary to interpolate between the data points to drive the texture model according to the operator's current speed and force. In this paper, to evaluate the pure reproduction ability of the PEQ, bilinear interpolation, a traditional method in texture modeling, was implemented. In bilinear interpolation, the four nearest data points are used to calculate the parameters corresponding to the current location. Therefore, the number of interpolation equations depends on the number of peaks. One peak requires four equations, two peaks require seven, and three require ten. However, from the results of multiple regression analysis, a simpler complementary method can be applied in the future.

C. VIBRATION FEEDBACK

Interpolation equations provide PEQ parameters corresponding to the current operating state. These parameters define the characteristics of the current PEQ. White noise is generated in real time and filtered by the designed PEQ, producing texture vibrations according to the model. These texture vibrations are output as voltage signals from the microcontroller and drive the vibrator according to the voltage. However, this approach assumes that the vibrator has ideal characteristics. The vibrator's ability to reproduce vibrations decreases as the frequency deviates from the resonance point. Therefore, it is necessary to apply an inverse filter to cancel out the resonant characteristics.

Our vibrator used is a Vibrotransducer Vp416 from Acouve Labs. The characteristics of the vibrator were recorded by placing it on a sponge and measuring it with the ADcmXL3021 accelerometer. The test signal, white noise at maximum amplitude, was played back to visualize the full-band reproduction characteristics. A notch filter $H_{\mathrm{BEF}}(z)$ was applied to the waveform to pass frequencies other than the resonance point based on the frequency, amplitude, and bandwidth at the resonance point. The resonance features of the peaks were analyzed using the same procedure used for modeling. The inverse filter formula is as follows:

$$\tilde{a}(z) = G_o\hat{a}(z) + G_{\mathrm{BEF}}H_{\mathrm{BEF}}(z)\hat{a}(z) \tag{7}$$

where G_{BEF} is the gain applied to the waveform after the notch filter, and G_o is the gain applied to the waveform before the filter. Combining these two waveforms compensates for the decrease in amplitude away from the resonance point. This process enables the output of the texture model-specific characteristics from the vibrator.

VII. EXPERIMENTAL METHOD

In this section, the methodologies employed to evaluate the reproducibility of the simplified texture models developed in this research are described. The evaluation consisted of two subjective tests, absolute and relative, conducted to verify the efficacy of the simplified texture models. The Human Life Ethics Committee at Tokyo Denki University approved

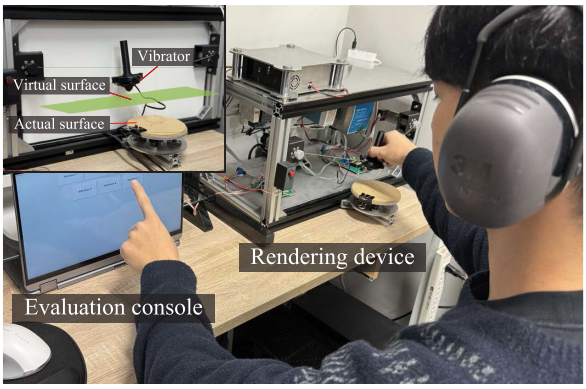

FIGURE 8. Experimental setup for subjective evaluation. The entire apparatus is visible to the subject. Subjects could touch the real surface by pressing the red button to turn off the virtual surface.

the experiments, ensuring ethical compliance throughout the study.

A. APPARATUS

In the experimental setup, a cable-linked force feedback device is utilized to generate surface reaction forces. The device comprises two motors spaced 600 mm apart, with the force feedback mediated through cables (Fig. 8). The workspace was up to 200 mm from the center, and the virtual surface was 50 mm below the motor position. An actual surface, mounted on springs capable of a 10 mm extension, is positioned 80 mm below the virtual surface. This placement allows for the presentation of a virtual surface with spring characteristics similar to those of the actual surface, ensuring consistency in haptic feedback.

A button is placed on the side of the device, allowing subjects to toggle the virtual surface on and off, allowing direct comparison with the actual surface. The experimental console for subject evaluation is set up on a laptop that is used to manage the texture presentation order and record selected answers.

B. PROCEDURE

An initial training session was conducted to accommodate subjects unfamiliar with the haptic presentation device. This training was essential to ensure that the subjects stayed within the operational limits of the device. The training also included familiarization with the texture samples and the experimental tasks. The sequence of texture presentations was randomized using the Fisher-Yates algorithm. Therefore, the experimental order was unknown to the subjects and the experimenter to maintain objectivity.

1) ABSOLUTE EVALUATION

In the absolute evaluation, the participants were informed that the virtual surface presentations corresponded to the actual surface. They were asked to compare the virtual surface with the actual surface and the vibration magnitude and frequency similarity. The visual analog scale (VAS) was used for the evaluation, allowing for detailed subjective assessments [44], [45]. The subjects rated the similarity of the vibration amplitude and frequency patterns corresponding to the surfaces' perceived intensity and texture patterns. The evaluation covered all seven texture types used in the study. The presentation order and the sequence of virtual and actual surface interactions were randomized.

2) RELATIVE EVALUATION

In the relative evaluation, a forced choice method [46], where the subjects were presented with an actual surface and had to identify the corresponding virtual surface from seven options, is implemented. This 7-alternative forced-choice task assessed the ability of the subjects to match the virtual surfaces to the actual surface, resulting in a baseline chance level of 14 %. The selection was made on a laptop, with the chosen virtual surface presented upon button press. The subjects could freely switch between the actual and virtual surfaces to make comparisons and selections. This process was repeated three times for each texture sample, with the button layout and the surface randomly assigned in each session. The entire procedure was conducted for the complete and simplified texture models on different days and in a randomized order to prevent bias.

VIII. RESULTS

The simplified texture models were evaluated through subjective absolute and relative evaluations. Twenty subjects (18 males and 2 females in their 20s) participated in the absolute evaluation experiment. Twenty-four subjects (22 males and 2 females in their 20s) participated in the relative evaluation experiment. None of the subjects had specific illnesses and could adequately determine the tactile perceptions. The subjects could refuse to participate in any stage of the experiment, depending on their physical condition. They could also take breaks to recover from numbness in their fingers. Both experiments were completed in approximately 30 minutes per trial, and the subjects were not restrained for long periods.

A. ABSOLUTE EVALUATION

The data were averaged across subjects, and the results were presented as the mean values and standard error bars (Fig. 9). A paired t-test was applied to compare the perceived similarities before and after simplification of the texture models.

Strong significant differences were observed for the vibration magnitude similarity for *PVC* and *leather*, indicating a notable perception change due to the simplification process. Other textures did not show significant differences, suggesting that the simplification did not markedly affect the perceived similarity. Most textures, except *aluminum*, scored above 50 % in similarity at the pre-simplification stage.

Frequency similarity followed a similar trend, and most textures did not show significant differences after simplification, except for *PVC*. However, *leather* showed a lower similarity score even before simplification, and a slight but significant difference was observed for *canvas* post-simplification. Despite this, the similarity remained high for

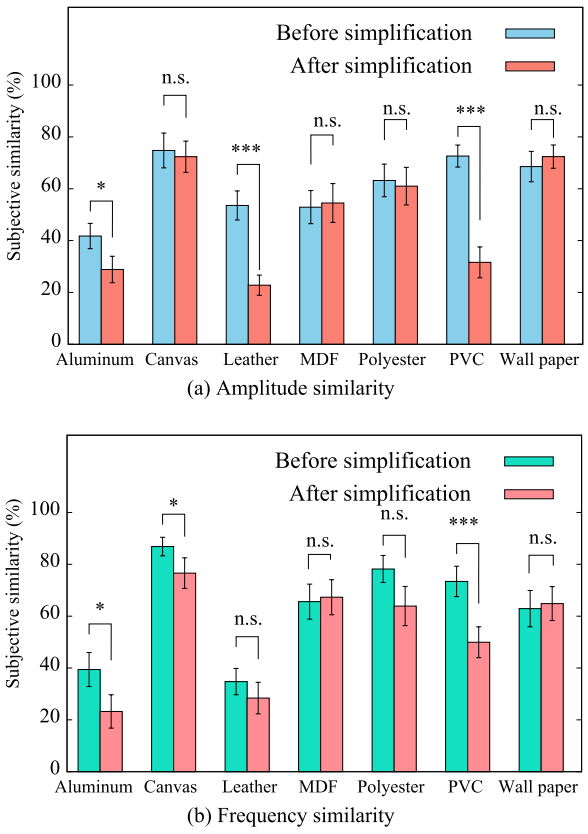

FIGURE 9. These are the results of the subjective evaluation using the VAS. (a) The similarity of the stimulus magnitude and (b) the frequency similarity. The reduction in roughness layers for either item did not affect most textures.

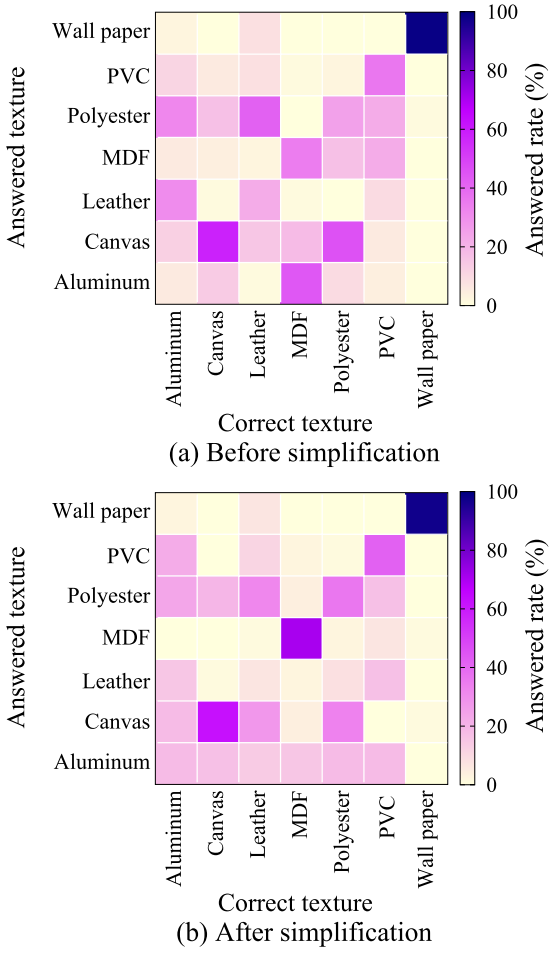

FIGURE 10. The confusion matrices of the 7-alternative forced-choice task. (a) The case where all peaks are reproduced. (b) The case where the peaks below the ADT are reduced.

canvas, indicating a minor perceptual impact due to the simplification.

B. RELATIVE EVALUATION

The 7-alternative forced-choice task was repeated three times for each texture under complete and simplified model conditions, with the sequence randomized. Correct matches were plotted in a confusion matrix, and the diagonal represents accurate selections (Fig. 10).

Errors showed patterns, with *canvas* and *polyester* often being confused with each other over chance level. *Aluminum* did not exhibit a consistent misidentification pattern. After simplification, the range of textures misidentified as *aluminum* expanded, suggesting a general shift in perceptual attributes due to simplification.

Only the correct rates are compared, as shown in Fig. 11. The t-test was performed in the same way as in Subsection VIII-A. For *wall paper*, most subjects could select an answer without error. *canvas* also had a correct response rate of approximately 60 %, while others had a response rate less than 40 %. *MDF* exceeded 60 % under the simplification condition. The only significant change was in the *MDF*, with little difference in the others. Compared to

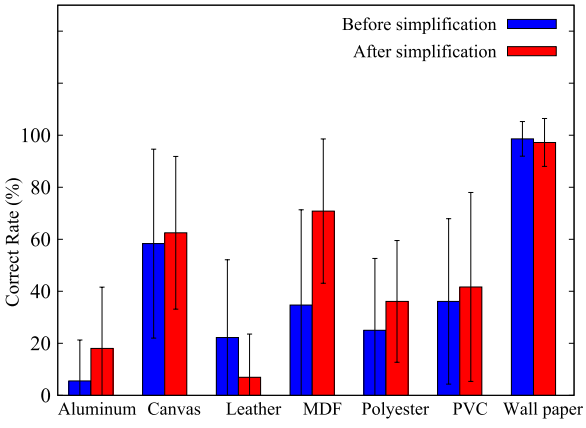

FIGURE 11. Comparisons were made before and after reducing the roughness layer concerning the percentage of correct responses. The error bars represent the standard errors between the subjects. It can be seen that only the *MDF* has a large variation.

the chance level, *aluminum* before reduction and *leather* after reduction were below the chance level.

IX. DISCUSSION

The aim of this subjective evaluation is to validate our simplification approach through absolute and relative assessments. The results indicate that the selective elimination of imperceptible roughness layers from the texture models does not significantly compromise their perceived similarity to actual textures. In this section, the results obtained from our experiments and the feasibility of the texture models based on multiple regression models are discussed.

A. EVALUATION OF PEAK ELIMINATION

The ability to selectively omit non-perceptible roughness layers without affecting perceived similarity is a significant finding. These results suggest that the criteria for determining the perceptual threshold based on the ADT were generally adequate, although there is some need for more consideration.

PVC and *leather* showed notable differences in perceived vibration magnitude after simplification. The decrease in perceived similarity for specific textures shows the need for a more conservative approach to defining the simplification threshold. Due to their randomness, the white noise used for the simplification process and experiments is not entirely the same wave. The variation could have caused the amplitude of some textures near the boundary to be above the threshold. Sample vibrations of about one second were used for the simplification process, but a longer span of samples was needed.

B. REGRESSION MODEL-BASED VIBRATION GENERATION FEASIBILITY

The results of both subjective evaluations suggest that perceived differences, particularly for the amplitude, were more pronounced than for frequency. This result implies that while the overall vibration intensity might change as a result of simplification, the removed specific frequency components were not identified. This observation is crucial for considering regression model-based approaches. Therefore, a detailed model for each peak might be optional for texture vibration generation. Instead, focusing on the spectral centroid's response to the velocity and deriving the individual peak characteristics from this overarching trend could be a more efficient strategy.

C. LIMITATIONS

In this study, we did not account for temporal variations, which can be significant for inhomogeneous textures. The impact of temporal variations may not be needed for applications primarily concerned with material selection or surface treatment in texture authoring. However, additional methods for capturing these aspects would be necessary for applications where precise temporal dynamics are crucial.

Furthermore, the regression analysis provided insights into the physical interactions captured by the texture models. However, a direct model between physical texture properties (e.g., roughness and hardness) and model parameters remains to be fully established. Future research could involve creating regression models for textures with known physical properties, thereby creating a texture authoring system based on physical texture properties.

X. CONCLUSION

In this research, we presented a novel approach to creating texture models using PEQ techniques. The texture models were constructed on the basis of frequency, amplitude, bandwidth, and noise ratio parameters, which have physical significance. Additionally, a simplified modeling approach was introduced to improve authoring and rendering efficiency based on physical and perceptual rules.

Subjective evaluations, comprising both absolute and relative evaluations, confirmed the effectiveness of the simplification approach. It was demonstrated that excluding imperceptible roughness layers did not significantly diminish the perceived similarity of the texture models to actual textures. This finding has practical implications for texture modeling, making it more efficient while maintaining essential perceptual qualities.

This research also showed the potential of regression analysis in modeling texture vibrations, revealing insights into the relationship between surface interactions and vibration properties. This knowledge could provide more streamlined texture authoring approaches, particularly in material selection and surface treatment.

In conclusion, this study contributes to tactile texture modeling by offering a method that efficiently reproduces actual textures while reflecting the fundamental principles of surface interactions. The results have promising applications in texture authoring and material selection in the industrial field.

REFERENCES

[1] R. L. Klatzky, S. J. Lederman, C. Hamilton, M. Grindley, and R. H. Swendsen, "Feeling textures through a probe: Effects of probe and surface geometry and exploratory factors," *Perception Psychophys.*, vol. 65, no. 4, pp. 613–631, May 2003.

[2] M. Konyo, S. Tadokoro, A. Yoshida, and N. Saiwaki, "A tactile synthesis method using multiple frequency vibrations for representing virtual touch," in *Proc. IEEE/RSJ Int. Conf. Intell. Robots Syst.*, Aug. 2005, pp. 3965–3971.

[3] S. Choi and H. Z. Tan, "Toward realistic haptic rendering of surface textures," *IEEE Comput. Graph. Appl.*, vol. 24, no. 2, pp. 40–47, Mar. 2004.

[4] S. J. Bensmaia and M. Hollins, "Complex tactile waveform discrimination," *J. Acoust. Soc. Amer.*, vol. 108, no. 3, pp. 1236–1245, Sep. 2000.

[5] H. Vasudevan and M. Manivannan, "Recordable haptic textures," in *Proc. IEEE Int. Workshop Haptic Audio Vis. Environments Their Appl. (HAVE)*, Nov. 2006, pp. 130–133.

[6] V. L. Guruswamy, J. Lang, and W.-S. Lee, "Modelling of haptic vibration textures with infinite-impulse-response filters," in *Proc. IEEE Int. Workshop Haptic Audio Vis. Environments Games*, Nov. 2009, pp. 105–110.

[7] J. M. Romano and K. J. Kuchenbecker, "Creating realistic virtual textures from contact acceleration data," *IEEE Trans. Haptics*, vol. 5, no. 2, pp. 109–119, Apr. 2012.

[8] H. Culbertson, J. Unwin, and K. J. Kuchenbecker, "Modeling and rendering realistic textures from unconstrained tool-surface interactions," *IEEE Trans. Haptics*, vol. 7, no. 3, pp. 381–393, Jul. 2014.

[9] W. Nai, J. Liu, C. Sun, Q. Wang, G. Liu, and X. Sun, "Vibrotactile feedback rendering of patterned textures using a waveform segment table method," *IEEE Trans. Haptics*, vol. 14, no. 4, pp. 849–861, Oct. 2021.

[10] S. Shin, R. H. Osgouei, K.-D. Kim, and S. Choi, "Data-driven modeling of isotropic haptic textures using frequency-decomposed neural networks," in *Proc. IEEE World Haptics Conf. (WHC)*, Jun. 2015, pp. 131–138.

[11] J. B. Joolee and S. Jeon, "Deep multi-modal network based data-driven haptic textures modeling," in *Proc. IEEE World Haptics Conf. (WHC)*, Jul. 2021, p. 1140.

[12] W. Hassan, A. Abdulali, M. Abdullah, S. C. Ahn, and S. Jeon, "Towards universal haptic library: Library-based haptic texture assignment using image texture and perceptual space," *IEEE Trans. Haptics*, vol. 11, no. 2, pp. 291–303, Apr. 2018.

[13] Y. Ujitoko, Y. Ban, and K. Hirota, "GAN-based fine-tuning of vibrotactile signals to render material surfaces," *IEEE Access*, vol. 8, pp. 16656–16661, 2020.

[14] N. Heravi, W. Yuan, A. M. Okamura, and J. Bohg, "Learning an action-conditional model for haptic texture generation," in *Proc. IEEE Int. Conf. Robot. Autom. (ICRA)*, May 2020, pp. 11088–11095.

[15] W. Hassan, A. Abdulali, and S. Jeon, "Authoring new haptic textures based on interpolation of real textures in affective space," *IEEE Trans. Ind. Electron.*, vol. 67, no. 1, pp. 667–676, Jan. 2020.

[16] S. Lu, M. Zheng, M. C. Fontaine, S. Nikolaidis, and H. Culbertson, "Preference-driven texture modeling through interactive generation and search," *IEEE Trans. Haptics*, vol. 15, no. 3, pp. 508–520, Jul. 2022.

[17] J. Li and Y. Zhang, "Ceramic product design based on bump texture mapping," in *Proc. 4th Int. Conf. Intell. Human-Mach. Syst. Cybern.*, vol. 1, Aug. 2012, pp. 21–24.

[18] T. Kanemoto, Y. Kurita, and K. Imaoka. (2012). *Tactile Digital Design Tool That Predicts Tactile Sensation From Height Map Data*. Accessed: Oct. 2, 2023. [Online]. Available: https://www.bsys.hiroshima-u.ac.jp/kurita/work_j_digitalhapt2022.html

[19] S. Kuroki, M. Sawayama, and S. Nishida, "The roles of lower- and higher-order surface statistics in tactile texture perception," *J. Neurophysiol.*, vol. 126, no. 1, pp. 95–111, 2021.

[20] C. G. McDonald and K. J. Kuchenbecker, "Dynamic simulation of tool-mediated texture interaction," in *Proc. World Haptics Conf. (WHC)*, Apr. 2013, pp. 307–312.

[21] J. Hu, X. Zhang, X. Yang, R. Jiang, X. Ding, and R. Wang, "Analysis of fingertip/fabric friction-induced vibration signals toward vibrotactile rendering," *J. Textile Inst.*, vol. 107, no. 8, pp. 967–975, 2016.

[22] M. Strese, C. Schuwerk, A. Iepure, and E. Steinbach, "Multimodal feature-based surface material classification," *IEEE Trans. Haptics*, vol. 10, no. 2, pp. 226–239, Apr. 2017.

[23] S. J. Lederman, "Tactile roughness of grooved surfaces: The touching process and effects of macro- and microsurface structure," *Perception Psychophys.*, vol. 16, no. 2, pp. 385–395, Mar. 1974.

[24] M. Hollins and S. R. Risner, "Evidence for the duplex theory of tactile texture perception," *Perception Psychophys.*, vol. 62, no. 4, pp. 695–705, Jan. 2000.

[25] K. Johnson, "The roles and functions of cutaneous mechanoreceptors," *Current Opinion Neurobiol.*, vol. 11, no. 4, pp. 455–461, Aug. 2001.

[26] K. Tozuka and H. Igarashi, "Effects on perception when removing one frequency component from two harmonic vibrations," in *Proc. IEEE World Haptics Conf. (WHC)*, Jul. 2023, pp. 425–431.

[27] I. Hwang, J. Seo, and S. Choi, "Perceptual space of superimposed dual-frequency vibrations in the hands," *PLoS ONE*, vol. 12, no. 1, Jan. 2017, Art. no. e0169570.

[28] S. Okamoto and Y. Yamada, "Lossy data compression of vibrotactile material-like textures," *IEEE Trans. Haptics*, vol. 6, no. 1, pp. 69–80, 1st Quart., 2013.

[29] R. Hassen, B. Gülecyüz, and E. Steinbach, "PVC-SLP: Perceptual vibrotactile-signal compression based-on sparse linear prediction," *IEEE Trans. Multimedia*, vol. 23, pp. 4455–4468, 2021.

[30] R. Hassen and E. Steinbach, "Subjective evaluation of the spectral temporal SIMilarity (ST-SIM) measure for vibrotactile quality assessment," *IEEE Trans. Haptics*, vol. 13, no. 1, pp. 25–31, Jan. 2020.

[31] A. Noll, C.-D. Curiac, B. Gülecyüz, and E. Steinbach, "Adaptive equalization of vibrotactile actuators," *IEEE Trans. Haptics*, vol. 14, no. 2, pp. 371–383, Apr. 2021.

[32] U. A. Alma and E. Altinsoy, "Perceived roughness of band-limited noise, single, and multiple sinusoids compared to recorded vibration," in *Proc. IEEE World Haptics Conf. (WHC)*, Jul. 2019, pp. 337–342.

[33] J. Kirsch, A. Noll, M. Strese, Q. Liu, and E. Steinbach, "A low-cost acquisition, display, and evaluation setup for tactile codec development," in *Proc. IEEE Int. Symp. Haptic, Audio Vis. Environments Games (HAVE)*, Sep. 2018, pp. 1–6.

[34] T. Murakami, F. Yu, and K. Ohnishi, "Torque sensorless control in multidegree-of-freedom manipulator," *IEEE Trans. Ind. Electron.*, vol. 40, no. 2, pp. 259–265, Apr. 1993.

[35] W. McMahan, J. M. Romano, A. M. A. Rahuman, and K. J. Kuchenbecker, "High frequency acceleration feedback significantly increases the realism of haptically rendered textured surfaces," in *Proc. IEEE Haptics Symp.*, Mar. 2010, pp. 141–148.

[36] Jeremy A. Fishel and Gerald E. Loeb, "Bayesian exploration for intelligent identification of textures," *Frontiers Neurorobot.*, vol. 6, p. 4, Jun. 2012.

[37] A. M. Okamura, J. T. Dennerlein, and R. D. Howe, "Vibration feedback models for virtual environments," in *Proc. IEEE Int. Conf. Robot. Automat.*, vol. 1, May 1998, pp. 674–679.

[38] H. Culbertson, J. M. Romano, P. Castillo, M. Mintz, and K. J. Kuchenbecker, "Refined methods for creating realistic haptic virtual textures from tool-mediated contact acceleration data," in *Proc. IEEE Haptics Symp. (HAPTICS)*, Mar. 2012, pp. 385–391.

[39] J. Romero, A. Garcia-Beltrán, and J. Hernández-Andrés, "Linear bases for representation of natural and artificial illuminants," *J. Opt. Soc. Amer. A, Opt. Image Sci.*, vol. 14, no. 5, p. 1007, 1997.

[40] S. Shin and S. Choi, "Hybrid framework for haptic texture modeling and rendering," *IEEE Access*, vol. 8, pp. 149825–149840, 2020.

[41] M. I. Awan, T. Ogay, W. Hassan, D. Ko, S. Kang, and S. Jeon, "Model-mediated teleoperation for remote haptic texture sharing: Initial study of online texture modeling and rendering," in *Proc. IEEE Int. Conf. Robot. Autom. (ICRA)*, May 2023, pp. 12457–12463.

[42] H. Culbertson and K. J. Kuchenbecker, "Importance of matching physical friction, hardness, and texture in creating realistic haptic virtual surfaces," *IEEE Trans. Haptics*, vol. 10, no. 1, pp. 63–74, Jan. 2017.

[43] Y. Hirata and M. Sato, "3-dimensional interface device for virtual work space," in *Proc. IEEE/RSJ Int. Conf. Intell. Robots Syst.*, vol. 2, Jul. 1992, pp. 889–896.

[44] R. S. Johansson and G. Westling, "Signals in tactile afferents from the fingers eliciting adaptive motor responses during precision grip," *Exp. Brain Res.*, vol. 66, no. 1, pp. 141–154, Mar. 1987.

[45] I. Birznieks, P. Jenmalm, A. W. Goodwin, and R. S. Johansson, "Encoding of direction of fingertip forces by human tactile afferents," *J. Neurosci.*, vol. 21, no. 20, pp. 8222–8237, Oct. 2001.

[46] S. BensmaÏa, M. Hollins, and J. Yau, "Vibrotactile intensity and frequency information in the pacinian system: A psychophysical model," *Perception Psychophys.*, vol. 67, no. 5, pp. 828–841, Jul. 2005.

KEISUKE TOZUKA (Graduate Student Member, IEEE) received the B.S. and M.S. degrees in electronic system engineering from Tokyo Denki University, Tokyo, Japan, in 2018 and 2022, respectively, where he is currently pursuing the Ph.D. degree with the Department of Electronic System Engineering. He is doing research assistantship with Tokyo Denki University.

HIROSHI IGARASHI (Member, IEEE) received the B.S., M.S., and Ph.D. degrees from the Department of Electrical Engineering, Tokyo Denki University, in 2000, 2002, and 2005, respectively. He is currently an Associate Professor with the Department of Electrical and Electronic Engineering, Tokyo Denki University. His primary research interests include robotics, human–machine systems, and artificial intelligence. He is a member of IEEJ and JSME.